Int. J. Electrochem. Sci., 16 **(2021)** Article ID: 210325, doi: 10.20964/2021.03.34

International Journal of
ELECTROCHEMICAL
SCIENCE
www.electrochemsci.org

Valorization of biomass waste from yellow horn (*Xanthoceras sorbifolia*) through the preparation of porous carbon for supercapacitors

Fenfang Luo, Yves Iradukunda, Kaiqiang Yi, Yawen Hu, Xin Li, Guoying Wang, Gaofeng Shi[*]

School of Petrochemical Engineering, Lanzhou University of Technology, Lan gong ping Road, Lanzhou, Gansu, China
[*]E-mail: 1538601086@qq.com

Received: 9 November 2020 / *Accepted:* 18 December 2020 / *Published:* 31 January 2021

Hot trends have always been the successful production of green energies and the promotion of the added value of agricultural goods. In this research, we introduced a new type of porous carbon material which, after extracting oil from the Yellowhorn for high-performance supercapacitors, uses H_3PO_4 as an activator and is made from biomass waste. To date, experiments on nitrogen adsorption/desorption indicate that H_3PO_4-activated bio-carbon has strong pore-forming potential, while the basic surface area is 1530.18 m^2/g. The average pore volume of is 0.97 cm^3/g. In contrast, carbon content electrochemical efficiency demonstrates a high specific capacitance of 246.5 F / g in 6 M KOH aqueous solution at 1A/g. However, a high energy density of 34.24Wh/kg is also provided by the proposed symmetrical supercapacitor. at a density of 500 W/kg of power. The above results thus suggest that the by-product of biomass waste is an outstanding substitute material for high-performance supercapacitor preparation.

Keywords: Yellowhorn; bio-carbon; supercapacitors; electrochemical performance

1. INTRODUCTION

Human populations face enormous problems, such as global warming, air degradation, and fossil fuel extraction, which have drawn growing interest [1]. It is necessary to find alternatives for clean energy as well as energy storage equipment [2]. Supercapacitors, a novel rechargeable energy storage component [3] are of interest in many applications thanks to their favorable electrochemical properties including high power density, fast charge/discharge rate, and excellent cycle stability [4]. They have been widely applied in portable electronic devices, electric vehicles, the aerospace industry, and the military. Based on the energy storage mechanism, supercapacitors can be roughly chopped up into two categories: pseudo capacitor and electrochemical double-layer capacitor (EDLC) [5]. the fast-

reversible redox reactions in the electrodes have formed the capacitance in pseudo capacitor [6], as for EDLC, the energy is stored via by the adsorption/desorption of electrolyte ions on the surface of electrode materials [7], the representative materials of which is porous carbon [8].

As we all know, the characteristics of electrode materials play an important role in the performance of supercapacitors and the development of electrode materials is suitable for supercapacitors which is the key to improving the electrochemical performance of supercapacitors[9]. After decades of development, there are many kinds of electrode materials, which can be divided into carbon electrode materials, metal oxide electrode materials, conductive polymer electrode materials, and composite electrode materials [10]. According to the composition of electrode materials and compared with other supercapacitor electrode materials, carbon materials have relatively low prices and are most likely to be industrialized [11]. However, they have the advantages of stable chemical properties, developed pore structure, large specific surface area, and no pollution [12]. Yellowhorn (*Xanthoceras sorbifolia)* is a kind of edible oil tree species that grow well in cold, barren environments in China and seeds are rich in oil extraction [13]. About 55–65 % of the oil in the seeds is extracted for human consumption and about 35-45%of solid wastes are worthless [14]. The general treatment method was to compost or make feed, but the economic value of these two treatment methods was not effective due to the gases formed from landfills which can cause environmental pollution problems [15]. Based on this point of view, turning the yellow horn wastes into new energy storage materials can not only alleviate the energy crisis but also reduce the pollution caused by landfills. However, the purpose of this project was to report a simple technology that uses H_3PO_4 as an activator to prepare bio-carbon materials which are effective for supercapacitors. Hence, the results show that the ratio of activator has a great influence on the microstructure of the prepared carbon material and the electrochemical performance of the carbon material.

2. EXPERIMENTAL

2.1 Materials and reagents

Yellowhorn was obtained from jing mao company(Gansu, China), hydrochloric acid, Phosphoric acid, Acetylene Black, polytetrafluoroethylene (PTFE) solution (60%), Nickel foam (2 cm * 1 cm)

2.2 experimental methods

After extracting oil from Yellowhorn, the waste residue was crushed into a powder with a grinder and pushed through a 100-mesh sieve. The pulverized powder was used as a raw material for preparing bio-carbon and H_3PO_4 was an activator. Firstly, using phosphoric acid to impregnate the powder for 24 hours, then dry the mixture in an oven, put the dried solid mixture in a tube furnace for 2 hours at the temperature of 800℃ with the increasing and decreasing rate of 5℃/min, carbonize it under nitrogen, after that put it on a magnetic stirrer and soak it with 2 M hydrochloric acid solution.

Stir at room temperature for 12 hours. Finally, drying it for 12 hours at 70 °C in a vacuum oven, the porous carbon was collected. The porous carbon is denoted herein according to the expression PAC-X, where PAC-1 means that the solid powder to phosphoric acid mass ratio was 1:0, PAC-2 was 1:1, PAC-3 was 1:2, and PAC-4 was 1:3, PAC-5 was 1:4.

2.3 Test of electrochemical properties

The electrochemical performance test was conducted on the CHI660E electrochemical workstation with three electrodes, and the electrolyte was a 6 M KOH solution. According to the mass ratio of 80 percent, 15 percent, and 5 percent, the prepared porous carbon was combined with acetylene black and PTFE, and then coated the well-mixed slurry on the 2*1 cm nickel foam to cover the region of 1*1 cm, then placed at 80 ° C in a vacuum oven for drying over 12 hours, and then rendered electrode sheets under a pressure of 10 M Pa. As reference electrode and counter electrode, saturated calomel electrode (SCE) and platinum layer were used respectively, and on an electrochemical workstation, cyclic voltammetry (CV), constant current charge and discharge (GCD) and impedance (EIS) measurements were conducted. At scan rates ranging from $5mVs^{-1}$ to $100mVs^{-1}$, cyclic voltammetry (CV) measurements were performed. The calculation of constant current charge and discharge (GCD) was carried out at a current density of 1 A g^{-1} to 10 A g^{-1}. The voltage range measured by CV and GCD is both -1 to 0 V. The specific capacitance C (F·g-1), energy density E (W·h·kg-1) and power density P (W·kg-1) was calculated using the following formulae:

$$C = \frac{I\Delta t}{m\Delta V} \quad (1) \qquad E = \frac{1}{2} C\Delta V^{2} \quad (2) \qquad P = \frac{E}{t} \quad (3)$$

Δt (t) is the discharge time, m is the mass load, ΔV(V) is the potential window of discharge, E is the energy density and P is power density [16].

2.4 Structure characterization

Scanning electron microscopes (SEM, JSM-6701FJapan Electron Optics) and transmission electron microscopy (TEM, D-12489 Berlin, Am Studio 2D Germany) were used for analyzing the surface structure of the porous carbon. The pore size distribution and specific surface area of the samples were checked using the Brunauer-Em-mett-Teller (BET) for adsorption and desorption of nitrogen gas in a Micromeritics ASAP 2420 surface analyzer. To assess the crystal structure of the sample, the MSA-XD2 powder X-ray diffractometer (diffraction angle scanning range was 5 to 80 °) was used. A spectrometer (JYHR800, Micro-Raman) measured the Raman spectrum. X-ray photoelectron spectroscopy (XPS, PHI5702, and USA) was used to test the surface elemental composition.

3. RESULT AND DISCUSSION

3.1 SEM and TEM

SEM and TEM were used to analyze the surface morphology of samples PAC-1 and PAC-4. As shown in figure 1(a), the SEM image of PAC-1 shows an irregular plate-like morphology and relatively smooth surface, without obvious porous structure. After the activation process, the plate-like structure becomes interconnected porous carbon walls as shown in figure 1(b-c). These carbon walls contain randomly distributed uniform worm-like pores, forming an irregular 3D frame structure [17]. It is speculated that biochar and H_3PO_4 form a molten mixture during heating, and the reaction of H_3PO_4 with these oxygen-containing functional groups leads to the production of related sodium salt [18]. At high temperatures, these sodium salts will be pyrolyzed and then release gases such as CO_2 and H_2O. At the same time, the molten mixture will expand, forming an irregular porous structure when the gas escapes [19].

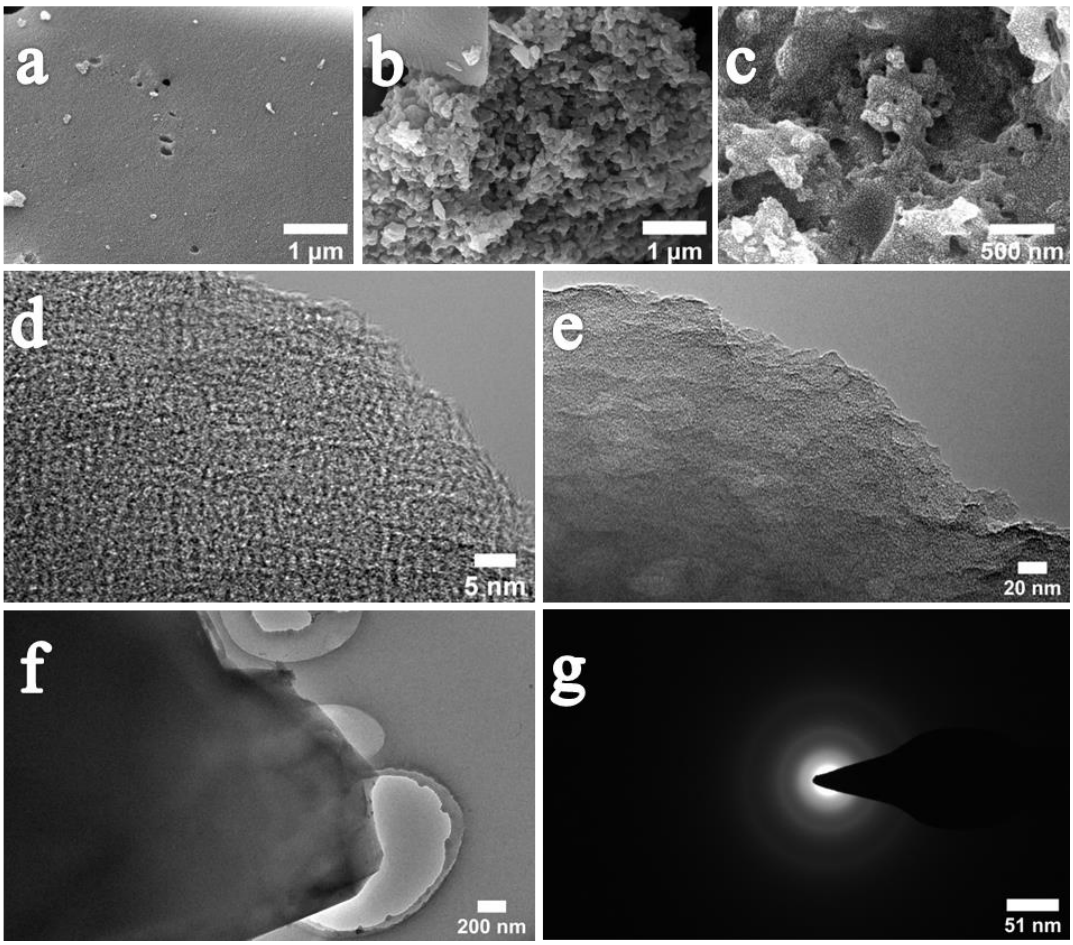

Figure 1. (a)SEM image of PAC-1; (b-c) SEM images of PAC-4; (d-f) TEM images of PAC-4; (g) the selected area diffraction pattern

3.2 XRD analysis of porous carbon

To analyze the crystal structure of the samples, XRD was used and the results are shown in figure 2. We used a D/max-2400C X-ray diffractometer (XRD) to perform XRD characterization on five samples. The diffraction source was Cu/K-a1, and the scanning range was 5 to 80 °. It can be seen from figure 2(a) that there are two broad characteristic peaks appear at 23.5 and 43.7, corresponding to the (002) crystal plane of the graphite layer and the (100) crystal plane of amorphous carbon, respectively [20,21]. Except for the diffraction peaks of carbon elements, no diffraction peaks of other elements were found, indicating that the carbon material prepared by this method has fewer impurities and high purity.

Raman analysis was performed on the sample and the results are shown in figure 2(b), two characteristic peaks can be observed. They are D peak and G peak, respectively. Where peak D represents the defect of the C lattice, and the peak G represents the in-plane stretching vibration of the SP^2 hybridization of the C atom [22]. The intensity ratio of peak D and peak G (I_D/I_G) can reflect the degree of disorder and graphitization of the structure in the material [23]. The I_D/I_G values of PAC-1, PAC-2, PAC-3, PAC-4, and PAC-5 were calculated to be 0.88, 0.93, 0.94, 0.96, and 0.89 respectively and the disorder degree of PAC-4 was the highest. This was because the activation process of phosphoric acid breaks the original carbon layer structure of the yellow horn powder, which makes the PAC-4 sample appears more abundant pore structure, but with the increase of the amount of phosphoric acid, the disorder of the sample and the generation of pores are decreasing, which was also consistent with the BET results.

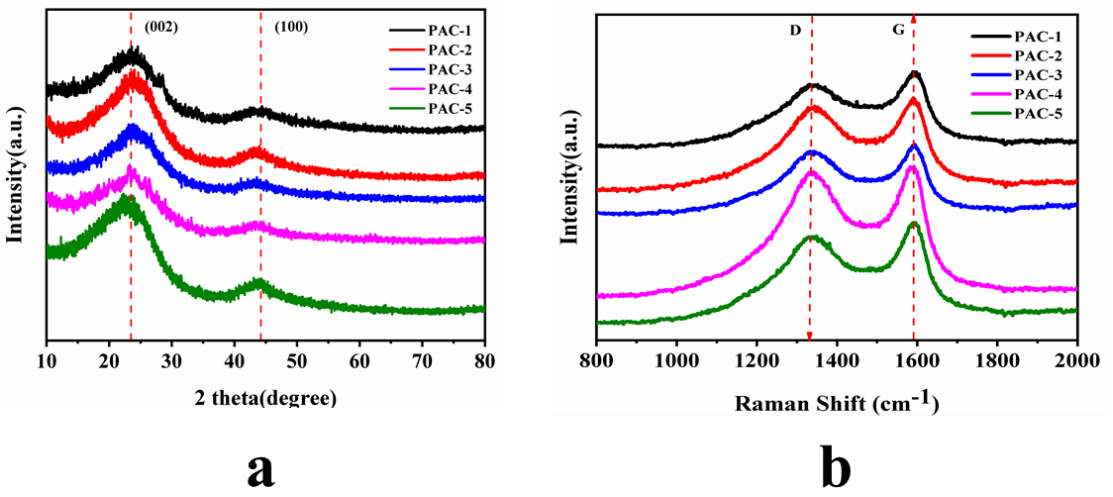

Figure 2. (a) XRD patterns of five samples; (b) Raman spectra of five samples

3.3 BET analysis of porous carbon

To analyze the specific surface area and pore structure of porous carbon, nitrogen adsorption-desorption was used, the isotherm of which is helpful to find whether it contains micropores (below 2

nm), mesopores (2-50 nm), or macropores (above 50 nm) [24]. The results are shown in figure 3. According to the International Union of Pure and Applied Chemistry (IUPAC) classification, porous carbon materials show a typical IV type of adsorption/desorption isotherm [25]. The slope and hysteresis loop varies with the amount of phosphoric acid added to the sample and the slope of the PAC-4 sample is higher than the other four samples, which indicates that it has a larger mesopores volume [26].

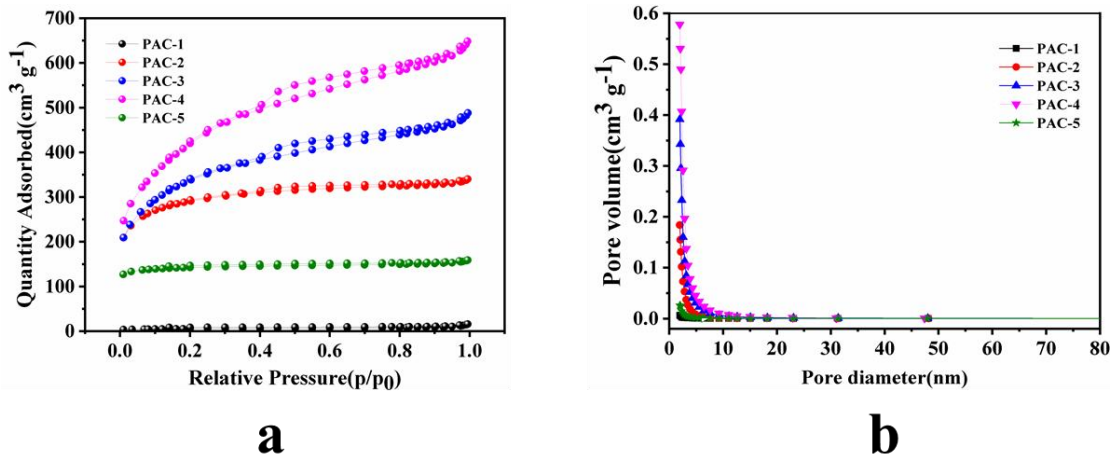

Figure 3. (a) N_2 adsorption/desorption isotherms and (b) the BJH pore size distribution curves of the porous carbons.

Table 1. The pore size distribution of porous carbon

Sample	S_{BET}/cm^2 g^{-1}	V_t/cm^3 g^{-1}	D_{ave}/nm	V_{mic}/cm^3 g^{-1}	V_{ext}/cm^3 g^{-1}	S_{mic}/cm^2 g^{-1}	S_{ext}/cm^2 g^{-1}
PAC-1	19.25	0.018	3.84	0.0017	0.0163	4.22	15.03
PAC-2	1002.89	0.52	2.06	0.26	0.26	559.89	443.00
PAC-3	1209.43	0.73	2.41	0.11	0.62	276.98	932.45
PAC-4	1530.18	0.97	2.54	0.04	0.93	130.28	1399.90
PAC-5	478.29	0.24	2.00	0.19	0.05	406.60	71.69

S_{BET}: surface area; V_t: total pore Volume; Dave: average pore diameter; V_{mic}: microspore volume; V_{ext}: external volume; S_{mic}: microspore surface area; S_{ext}: external surface area

Figure 3(b) shows the pore size distribution diagram tested by the Barrett-Joyner-Halenda (BJH) method. It can be observed that the pore size distribution of the sample after activation was about 2.5nm and the distribution was uniform. Through calculation, we obtained the specific surface area, the specific volume of mesopores, and the average pore diameter of each sample. The results are shown in Table 1. It can be seen from the table that the specific surface area of the sample PAC1-5 is

19.25 m^2g^{-1}, 1002.89 m^2g^{-1}, 1209.43 m^2g^{-1}, 1530.18 m^2g^{-1}, 478.29 m^2g^{-1}, respectively. The influence on the surface area value and the average pore diameter of the mass ratio (carbon/acid) are different. This is because the increased amount of phosphoric acid causes the clogging of pores due to the deposition of phosphate materials and other phosphor materials, thereby reducing the surface area value [27]. The five samples are all mesoporous structure, and the pore volume of PAC-4 was the largest, indicating that the material structure prepared by this method is mainly mesoporous, and the mass ratio of 1:4 (carbon/acid) was compared with other mass ratios. The obtained material has a well-developed pore structure. The total pore volume of PAC-4 is 0.97cm^3g^{-1}, and the mesopore volume is 0.937cm^3g^{-1}, accounting for 95.87% of the total pore volume.

3.4 XPS analysis of Porous carbon

To determine the electronic structure and surface composition of the sample surface, we performed an X-ray photoelectron spectroscopy (XPS) analysis. The contents of C, O, N, and P on the surface of the sample were 93.26% carbon, 6.55% oxygen, 0.19% nitrogen, and 0.00% phosphorus.

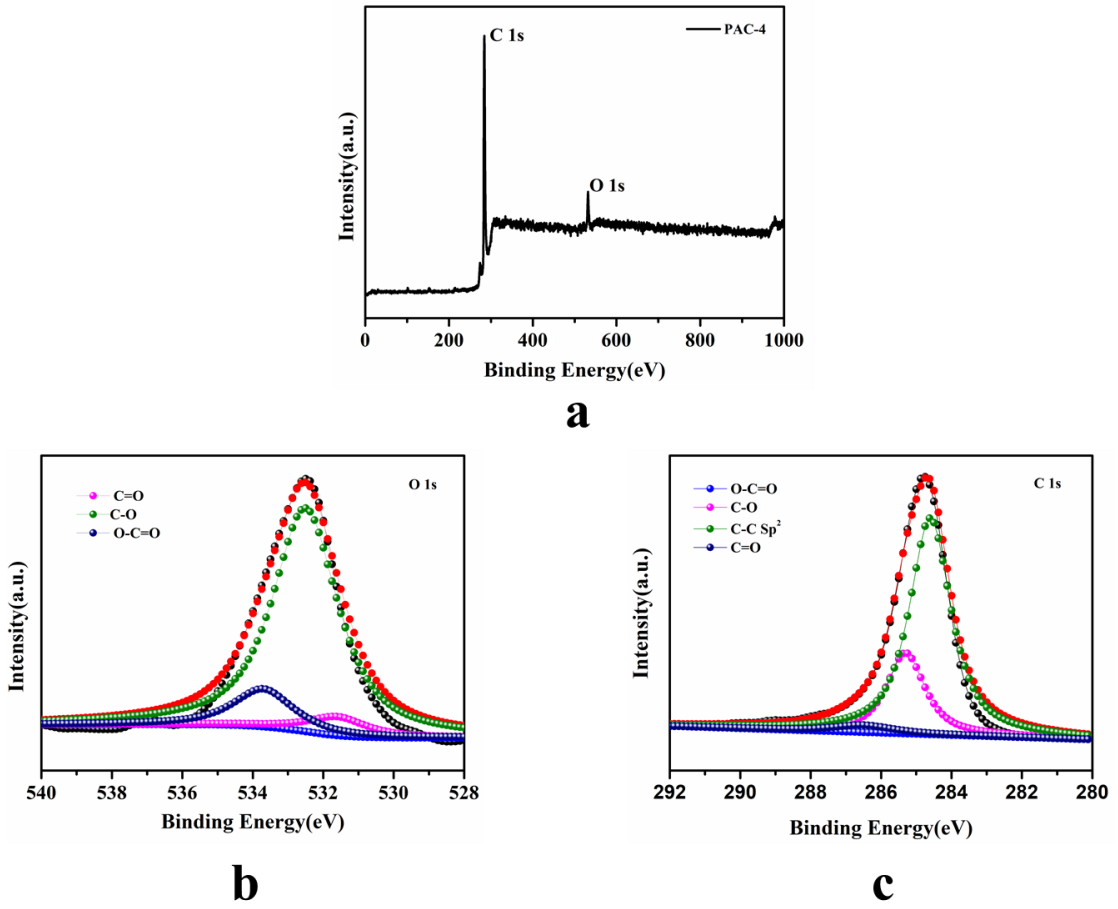

Figure 4. (a) XPS survey spectra of PAC-4, (b-c) C1s and O1s spectra of the PAC-4sample.

It shows that porous carbon does not contain nitrogen and phosphorus almost. Figure 4 is the spectrum of the PAC-4 sample and there are C peak and O peak. To further analyze the type and relative content of the functional groups of each element on the sample surface, we performed peak fitting on the C and O elements of the sample to obtain C1s, O1s spectra. Figure 4(b) is the C1s spectrum, Three different peaks located at ~284.6 eV[28], ~285.5 eV[29], and ~289.3 eV [30] correspond to the sp^2 hybrid (C=C, C-C), C-O bonding, and carboxyl or ester groups (O-C=O), respectively. For the O1s XPS spectrum, the sample can be fitted into three parts, as shown in figure(c). They are C=O at 531.6 eV, single-bonded oxygen (-O-) in the C-O group at 532.7 eV, and oxygen (O=C-O) in the carboxyl group at 533.7 eV [31].

3.5 electrochemical performance test

Figure 5(a) shows the cyclic voltammetry (CV) curve under different activator ratios, the voltage range was from -1 to -0V, and the scan rate was 5mV/s. It can be seen that the PAC-1sample prepared without H_3PO_4 shows a triangular-like CV and the rest of the samples are rectangular-like CV, and there is no obvious redox peak, showing an ideal double-layer capacitance, indicating that the capacitance of the sample is almost provided by carbon [32]. It was observed that as the amount of phosphoric acid activator increased, the surface of the enclosed area of the CV curve first increased and then decreased, indicating that the PAC-4 sample had the best electrochemical performance.

The galvanostatic charging-discharging (GCD) method is the most intuitive test method to show the performance of materials, and it is indispensable in the test. Figure 5(b) demonstrates the GCD curves at a current density of 1A g^{-1}. It can be seen that the GCD curve of each sample is in a symmetrical triangle shape, which indicates that the material has good electric double layer capacitance characteristics [33]. The specific capacitances of PAC-1, PAC-2, PAC-3, PAC-4, and PAC-5 at a current density of 1A g^{-1} are 101, 190.2, 201.9, 246.5, and 162.2 $F.g^{-1}$, respectively. with the increase of the activator, the GCD curve increases first and then decreases, which is consistent with the results of the CV test.

To understand the electrochemical performance of the five samples in-depth, impedance measurements (EIS) was carried out. The results are shown in figure 5(c), except for the sample PAC-1, the EIS of the other samples are all similar to a vertical straight line. And the sample PAC-4 has a more vertical Weber diffusion curve in the low-frequency region, which may be attributed to the difference in pore size distribution [21]. The approximately vertical Weber diffusion curve shows that sample PAC-4 has the best electron transport and diffusion properties among all samples.

Figure 5(d) depicts the CV curve of sample PAC-4 from 5 to 100 mV/sat different scan rates. The CV curves can still maintain a rectangular-like shape at a high scan rate, which indicates that the sample PAC-4 has good charge and discharge capabilities and excellent ion transport capabilities [16]. As the scanning rate increases, the deviation of the CV curve from the rectangle becomes larger. This is because the current response increases with the voltage change and the voltage change cannot be well balanced with the electrolyte diffusion speed in the electrode. Hence, it can only stay on the

surface or the large pores on the surface, resulting in a decrease in the effective surface area, an increase of the internal resistance of the capacitor, and a decrease in capacitance performance [34].

Figure 5(e) shows the GCD curves of PAC-4 under different current densities. As the current density increases from 1A.g^{-1} to 10 A.g^{-1}, the capacitance retention rate of PAC-1; PAC-2; PAC-3; PAC-4and PAC-5 was 52.16%, 76.23%, 76.52%, 78.9% and 72.74%, respectively. This was because there is a capacitance effect and an ohmic voltage drop and the ion cannot quickly pass through the diffusion channel inside the electrode under a large current. Thus, it takes a certain time to reach the steady-state formation.

Figure 5(g) proves the relationship between power density and energy density of porous carbon materials. Under the same current density, PAC-4 has the highest energy density. When the power density is 500W Kg^{-1}, the energy density is 34.24 Wh.Kg^{-1}, and when the power density is 5000W.Kg^{-1}, the energy density is 27.01 Wh.Kg^{-1}. Figure 5(h) shows the cycle characteristics of the PAC-4 sample at a current density of 1A.g^{-1}. It can be seen that after 5000 cycles of charge and discharge, the specific capacitance of the PAC-4 sample is 227 F g^{-1}, and the retention rate is 92.0%, indicating that the sample has good electrochemical cycling stability.

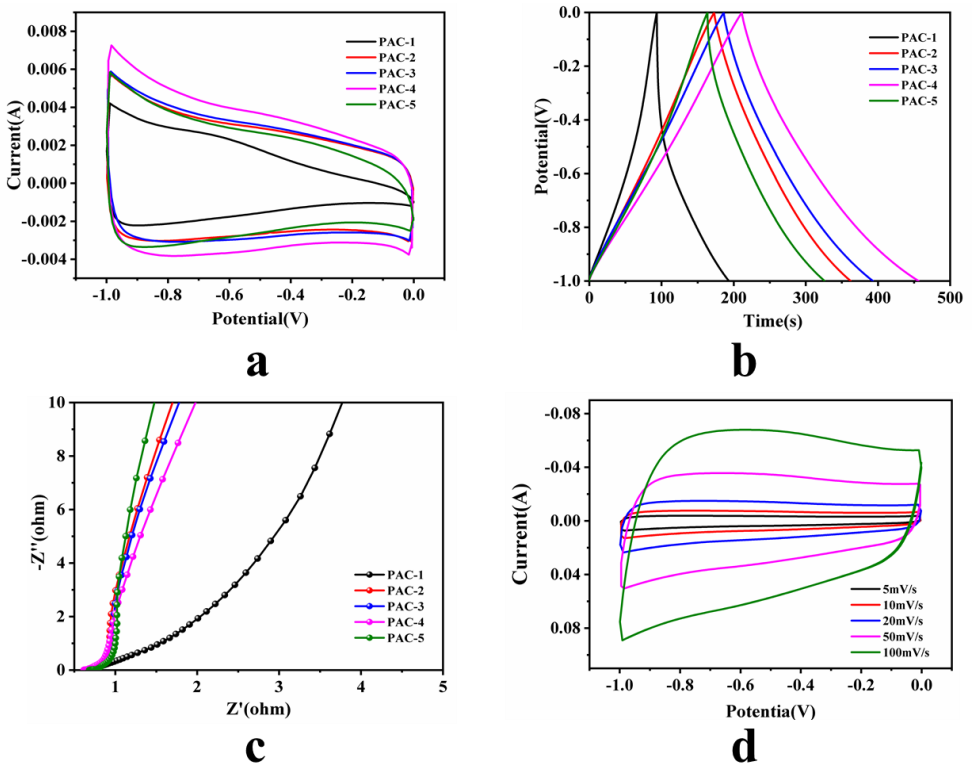

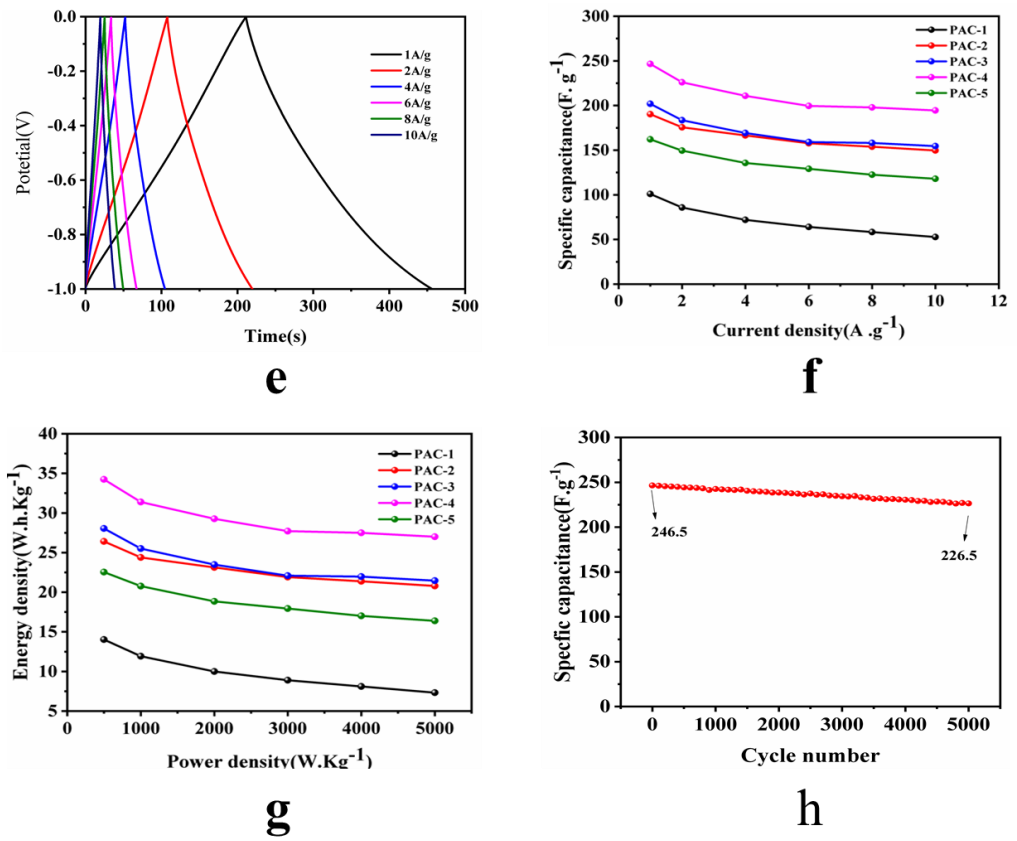

Figure 5. Electrochemical performance of the samples measured in a three-electrode system. (a) CV curves for all the samples at a scan rate of 5 $mV \cdot s^{-1}$; (b) GCD curves of all the samples at the current density of 1 $A.g^{-1}$; (c) EIS of all the samples; (d) CV curves for PAC-4 at scan rates ranging from 5 $mV.s^{-1}$ to 100 $mV.s^{-1}$ (e) GCD curves of PAC-4 at different current densities; (f)specific capacitance of the samples versus various current densities from 1 $A.g^{-1}$ to 10 $A.g^{-1}$;(g) power density; (h) PAC-4 in specific capacitance retention rates at the current density of 2 $A.g^{-1}$ after 5000 cycles.

Table 2. The specific capacitance of porous carbon ($F.g^{-1}$)

Current density ($A.g^{-1}$)	1	2	4	6	8	10
PAC-1	**101**	**85.8**	**72**	**64.1**	**58.3**	**52.7**
PAC-2	**190.2**	**175.6**	**166.4**	**157.7**	**153.8**	**145**
PAC-3	**201.9**	**183.6**	**169.2**	**159.1**	**158.2**	**154.5**
PAC-4	**246.5**	**226.0**	**210.8**	**199.5**	**198.0**	**194.5**
PAC-5	**162.2**	**149.6**	**135.6**	**129.1**	**122.6**	**118**

Table 3. Comparison of electrochemical performance of porous carbon with other different materials

Biomass precursor	Electrolyte	Specific capacity($F\ g^{-1}$) (current density)	Reference
Camellia pollen	**2M KOH**	**205 ($0.5\ A.g^{-1}$)**	**[1]**

Peanut shells	**1 M H_2SO_4**	**340 (0.25 A.g^{-1})**	**[2]**
Rice husks	**6 M KOH**	**233 (2 A.g^{-1})**	**[4]**
bean curd stick	**6 M KOH**	**405 (0.5 A.g^{-1})**	**[5]**
corn stalk core	**6 M KOH**	**323 (0.1 A.g^{-1})**	**[6]**
yellow horn	6 M KOH	246.5 (1 A.g-1)	This work

4. CONCLUSION

In summary, by using phosphoric acid as an activator and waste residue of the yellow horn, we have successfully prepared a porous carbon structure (PAC-4). A large specific surface area of 1530.18m2/g is revealed by PAC-4, pointing to excellent electrochemical efficiency, high specific capacitance, and excellent cyclic stability. PAC-4 showed a strong capacitance retention rate, while it was 78.9 % and the capacitance value stood at 92.0% after 5000 cycles of charging-discharging. This research therefore not only offers novel porous carbon content extracted from biomass for high-performance supercapacitor applications but can also bring tremendous additional value to yellow horn energy output.

ACKNOWLEDGEMENTS
This work was supported by the National Key R & D Program of China (No. 2016YFC0202900), the National Natural Science Foundation of China (No. 21567015, 21407072), the Natural Science Founda tion of Gansu Province (No. 18JR3RA079, 17JR5RA109), the Project of Food and Drug Administratio n of Gansu Province (No. 2018GSFDA014), the Gansu Provincial Party Committee Young Creative T alents (No. Ganzutongzi[2017]121), the Hongliu Science Fund for Distinguished Young Scholars (201 8), and Lanzhou University of technology Hongliu first-class discipline construction program.

References

1. C. Lu, Y. H. Huang, Y. J. Wu, J. Li and J. P. Cheng, *J. Power Sources*, 394 (2018) 9
2. Z. Xiao, W. Chen, K. Liu, P. Cui, and D. Zhan, *Int. J. Electrochem. Sci.*, 13 (2018) 5370
3. G. Lou, Y. Wu, X. Zhu, Y. Lu, S. Yu, C. Yang, H. Chen, C. Guan, L. Li, and Z. Shen, *ACS Appl. Mater. Interfaces*, 10 (2018) 42503
4. X. He, P. Ling, M. Yu, X. Wang, X. Zhang, and M. Zheng, *Electrochim. Acta*, 105 (2013) 635
5. L. Shi, L. Jin, Z. Meng, Y. Sun, C. Li and Y. Shen, *RSC Adv.*, 8 (2018) 39937
6. Y. Cao, K. Wang, X. Wang, Z. Gu, Q. Fan, W. Gibbons, J.D. Hoefelmeyer, P.R. Kharel, and M. Shrestha, *Electrochim. Acta*, 212 (2016) 839
7. G. Shi, Z. Wang, C. Liu, G. Wang, S. Jia, X. Jiang, Y. Dong, Q. Zhang, X. Li, and F.F. Luo, *Int.*

J. Electrochem. Sci., 14 (2019) 5259
8. D. Zhu, D. Mo, X. Ma, Q. Zhou, H. Liu, J. Xu, W. Zhou, and F. Zhao, *Synth. Met.*, 220 (2016) 155
9. Z. Teng, K. Han, J. Li, Y. Gao, M. Liand T. Ji, *Ultrason. Sonochem.*, 60 (2020) 104756.
10. C. Liu, G. Shi, G. Wang, P. Mishra, S. Jia, X. Jiang, P. Zhang, Y. Dong, and Z. Wang, *RSC Adv.*, 9 (2019) 6898
11. M. Conte, *Fuel Cells*, 10 (2010) 806
12. D. Tang, S. Hu, F. Dai, R. Yi, M.L. Gordin, S. Chen, J. Song, and D. Wang, *ACS Appl. Mater. Interfaces*, 8 (2016) 6779
13. Y. Liu, Z. Huang, Y. Ao, W. Li and Z. Zhang, *PLoS One*, 8 (2013) 1
14. Z. Shen, K. Zhang, Y. Ao, L. Ma, and J. Duan, *J. For. Res.*, 30 (2019) 869
15. G. Wang, Y. Iradukunda, G. Shi, P. Sanga, X. Niu and Z. Wu, *J. Environ. Sci.* (China), 99 (2021) 324
16. X. Hao, J. Wang, B. Ding, Y. Wang, Z. Chang, H. Dou and X. Zhang, *J. Power Sources*, 352 (2017) 34
17. J. Gao, J. Xie, X. Liu and H. Hu, *RSC Adv.*, 7 (2017) 20412
18. H. Wang, H. Wang, H. Zhao and Q. Yan, *Chem. Eng. J.*, 379 (2020) 122372.
19. J. Deng, T. Xiong, F. Xu, M. Li, C. Han, Y. Gong, H. Wang and Y. Wang, *Green Chem.*, 17 (2015) 4053
20. Y.L. Cao, L.F. Xiao, M.L. Sushko, W.Wang, B.Schwenzer, J. Xiao, Z.M. Nie, L.V. Saraf, Z.G. Yang and J. Liu, *Nano Lett.*, 12(2012) 3783.
21. S. Lei, L. Chen, W. Zhou, P. Deng, Y. Liu, L. Fei, W. Lu, Y.H. Xiao, and B.C. Cheng, *J. Power Sources*, 379 (2018) 74
22. X.L. Su, S.H. Li, S. Jiang, Z.K. Peng, X.X. Guan, and X.C. Zheng, *Adv. Powder Technol.*, 29 (2018) 2097
23. L. Zhang, Y. Jiang, L. Wang, C. Zhang, and S. Liu, *Electrochim. Acta*, 196 (2016) 189
24. J.R. Rajabathar, M. Sivachidambaram, J.J. Vijaya, H.A. Al-Lohedan and D.M.D. Aldhayan, *ACS Omega*, 5 (2020) 15028
25. H. Lu, W. Dai, M. Zheng, N. Li, G. Ji, J. Cao and *J. Power Sources*, 209 (2012) 243
26. X. Zhang, Y.P. Zheng, L.Lan and H.C. Yang, *New Carbon Mater.*, 29 (2014) 193
27. Y. Luo, D. Li, Y. Chen, X. Sun, Q. Caoanad X. Liu, *J. Mater. Sci.*, 54 (2019) 5008
28. D. Zhang, M. Han, Y. Li, J. He, B. Wang, K. Wang and H. Feng, *J. Power Sources*, 372 (2017) 260
29. Y. Zhou, R. Ma, S.L. Candelaria, J. Wang, Q. Liu, E. Uchaker, P. Li, Y. Chen and G. Cao, *J. Power Sources*, 314 (2016) 39
30. J. Zhou, Z. Zhang, W. Xing, J. Yu, G. Han, W. Si, and S. Zhuo, *Electrochim. Acta*, 153 (2015) 68
31. H. Chen, Y.C. Guo, F. Wang, G. Wang and F.Yu, *New Carbon Mater.*, 32 (2017) 592
32. F.J. García-Mateos, R. Ruiz-Rosas, J. María Rosas, E. Morallón, D. Cazorla-Amorós, J. Rodríguez-Mirasol, *T. Cordero and Sep. Purif. Technol.*, 241 (2020) 116724.
33. M.F. El-Kady, V. Strong, S. Dubin, and R.B. Kaner, *Science.*, 335 (2012) 1326
34. T. Eguchi, D. Tashima, M. Fukuma and S. Kumagai, *J. Clean. Prod.*, 259 (2020) 120822.